Hydrol. Earth Syst. Sci. Discuss., https://doi.org/10.5194/hess-2018-286
Manuscript under review for journal Hydrol. Earth Syst. Sci.
Discussion started: 12 July 2018

Hydrology and Earth System Sciences
Discussions

Variations of future precipitations in Poyang Lake Watershed under the global warming using a spatiotemporally distributed downscaling model

Ling Zhang [1], Xiaoling Chen[1, 2], Jianzhong Lu[1, *], Dong Liang[1]

[1]State Key Laboratory of Information Engineering in Surveying, Mapping and Remote Sensing, Wuhan University, Wuhan 430079, China

[2]Key Laboratory of Poyang Lake Wetland and Watershed Research, Ministry of Education, Jiangxi Normal University, Nanchang 330022, China

* *Correspondence to*: Jianzhong Lu (lujzhong@whu.edu.cn)

Abstract. Traditional statistic downscaling methods are processed on independent stations, which ignores spatial correlations and spatiotemporal heterogeneity. In this study, a spatiotemporally distributed downscaling model (STDDM) was developed. The method interpolated observations and GCMs (Global Climate Models) simulations to continual finer grids; then created relationship, respectively for each grid at each time. We applied the STDDM in precipitation downscaling of Poyang Lake Watershed using MRI-CGCM3 (Meteorological Research Institute Coupled Ocean-Atmosphere General Circulation Model3), with an acceptant uncertainty of ≤ 4.9%, and created future precipitation changes from 1998 to 2100 (1998-2012 in the historical and 2013-2100 in RCP8.5 scenario). The precipitation changes showed increasing heterogeneities in temporal and spatial distribution under the future climate warming. In the temporal pattern, the wet season precipitation increased with change rate (CR) = 7.33 mm/10a (11.66 mm/K) while the dry season precipitations decreased with CR = -0.92 mm/10a (-4.31 mm/K). The extreme precipitation frequency and intensity were enhanced with CR=0.49 days/10a and 7.2mm•day^{-1}/10a respectively. In the spatial pattern, precipitations in wet or dry season showed an uneven change rate over the watershed, and the wet or dry area exhibited a wetter or drier condition in the wet or dry season. Analysis with temperature increases showed precipitation changes appeared significantly ($p < 0.05$ and $R \geq 0.56$) correlated to climate warming. The results implicated the increasing risk of flood-droughts under global warming and were a reference for water balance analysis and water resource planting.

Hydrol. Earth Syst. Sci. Discuss., https://doi.org/10.5194/hess-2018-286
Manuscript under review for journal Hydrol. Earth Syst. Sci.
Discussion started: 12 July 2018

1 Introduction

Global warming has caused precipitation redistribution in temporal and spatial distribution (Frei et al. 1998; Trenberth et al. 2011), increasing the frequency and intensity of floods and droughts, thus seriously threating to social systems and ecosystems (Pall et al, 2000; Dai, 2013). To the fragile ecological and living environment, what the future hydrological situation will be under future global warming is a crucial question to avoid or reduce damages from climate warming.

As a basic tool in assessing future climate change effects, Global Climate Models (GCMs) provide an initial source of future climates (Xu, 1999). However, GCMs remain coarse with global resolutions larger than 1°×1°, which is unable to apply in regional scale as watersheds. Downscaling algorithms have been developed to link the global-scale GCMs outputs and regional-scale climate variables, including dynamic (Giorgi, 1990; Teutschbein and Seibert, 2012) and statistic (Wilby et al., 2007; Chu et al., 2010) models. The dynamic method employs regional climate models (RCMs) nested inside GCMs based on complex physics of atmospheric processes and involves high computational costs. Limited by an insufficient understanding of the physical mechanism and expensively computing resources, the dynamic downscaling model cannot easily satisfy small and mid-size region as Poyang Lake Basin. Unlike dynamic downscaling models, statistic downscaling constructed an empirical relationship between the global-scale output and local-scale climate variables with inexpensive computations. Benefitting from inexpensive computations and easy implementations, downscaling methods have been widely used, including regression models (Labraga et al. 2010, Quintana et al. 2010; Zorita et al. 1999), weather typing schemes (Boéj et al. 2007; ENKE et al. 2005) and weather generators (Mullan et al., 2016; Baigorria and Jones et al., 2011).

In these researches, statistical downscaling methods have been developed based on the relationship between the global-scale simulations and local observations in the station scale. The methods are processed on each station independently. Thus, the specific downscaling relationship and downscaled climate variable, are both independent and discrete in the station scale, instead of being spatially continuous in grid-scale with a finer resolution. However, as underlays of local region is complex with different topographies, land covers and clouds coverage, the downscaling relationships and downscaled climate variables at discrete stations can’t express the spatial heterogeneity clearly, compared to the spatially continuous data. Particularly, for the ungauged area without stations covered, it is inviable to get high-quality of downscaling relationships and local climates.

Moreover, local climate results and downscaling relationship in the station scale, are difficult to show the spatial correlation; whereas results from the downscaling which is processed on spatially continuous data such as grids, can show spatial relationship naturally. Additionally, spatially continuous data can be directly used in the spatially distributed hydrological model such as Crest (Wang et al., 2011), VIC (Lohmann et al. 1998), and MIKE SHE (DHI, 2014), which is the focus and frontier of international hydrological scientific research (Beven et al. 1990). Besides, downscaled climate data in spatially continuous pattern can be easily integrated with remote sensing data of geologies, topographies, soils, or land covers. In fact, spatially continuous data is widely used as remote sensing technology develops rapidly, which benefits hydrological models by providing data source (Engman et al., 1991). Therefore, downscaling method processed on spatially continuous data is of vital importance. The spatial distributed downscaling method, which creates downscaling relationship and project climates at spatial continuous scale, should be taken into consideration.

In addition to the spatial heterogeneity, the relationship between the climate variables of global-scale and local-scale also shows different in temporal heterogeneity of one year, as dominator affecting climate varies in different time (eg. seasons or Months). Therefore, the temporal distributed downscaling method, which creates different relationship at different time, should be taken into consideration. However, many downscaling methods didn't take temporal heterogeneity into consideration. For each individual observed site, the established downscaling method was global standard for the whole time series data, instead of being different in separate seasons or Months (Labraga 2010; Wu et al., 2017; Sachindra et al., 2018). In the study, the temporally distributed downscaling could be considered. Combining the heterogeneity in time and continual space, a climate downscaling model based on spatiotemporal distributed framework, a spatiotemporal distributed downscaling method, should be proposed to project future climate changes in regional scale.

Sensitive to climate changes in the East Asian monsoon region, Poyang Lake Watershed is not immune to global warming. Precipitation redistributions under global warming has caused more extreme hydrological events, with manifestation of the enhanced flood frequency and intensity (Wang et al., 2009; Guo et al., 2006), significant decline of lake level and inundation area (Feng et al. 2012; Zhang et al. 2014), which poses a threat to the fragile wetland and forest ecosystem (Han et al. 2015, Dyderski et al. 2018), economic developments and people's lives (Ye et al., 2011).

However, the Poyang Lake Wetland ecosystem, is an internationally important habitat for migratory birds, abundant of biodiversity and regarded as Natural Reserve; the watershed is commercial grain production area, an important part of Yangtze River Economic Belt. As a significant economic and ecosystem region, investigating the future precipitation changes in the watershed is crutial for prevention from climate damages. Previous studies of future precipitation changes in Poyang Lake Watershed includes temporal and special pattern. Precipitation changes in temporal pattern, focused on intensity and frequency of precipitation extremes (Hong et al. 2014; Wang et al. 2017), as well as annual or quarterly total precipitations (Guo et al., 2010; Guo et al., 2008; Li et al., 2016). In spatial pattern, precipitation change analysis is based on the five sub-basins (Xinjiang, Raohe, Xiushui, Ganjiang and Fuhe sub-basins) (Guo, et al. 2010; Hong, et al. 2014), 13 discrete metrological stations (Li et al. 2016), or 7 coarse grids (Guo, et al. 2008). Little research concerns on spatial-temporal distribution with continual finer grids space, not to mention the possible driving force analysis for precipitation changes related to increasing temperatures.

In the study, taking Poyang Lake Watershed as a test case, we projected future precipitations based on the spatiotemporal distributed downscaling method (STDDM), using MRI-GCM3 simulations and metrological observations, with the following specific objects: (1) developing a spatiotemporal distributed downscaling method (STDDM) for spatially continual future climate variables projections; (2) documenting precipitation changes in temporal and spatial pattern for Poyang Lake Watershed in the 21th century, and correlations between precipitation changes and temperature increasing. Future precipitation changes can provide basic hydrological information to get a better understanding of water resource volumes and flood-droughts risks, which benefits a scientific sight in wetland and forest ecosystem conservation, and aids decision making in development, utilization and planning of water resources.

2 Study area and datasets

2.1 Study Area

Poyang Lake Basin (24°28’-30°05’ N and 113°33’-118°29’E) is located in the southeast of China, connected with Yangtze River in the north (Fig 1). Within the southeast subtropical monsoon zone, the annual average temperature of the watershed is 17.5℃. The mean annual precipitation is 1638mm, with 192 rainy days (daily precipitation ≥ 0.1 mm/day）and 173 rain-free

days (daily precipitation < 0.1 mm/day). The rainy season lasts from April to July, about 70% of the annual total amount. Inter or intra annual precipitation variations are dominated by the southeast and southwest monsoon, mainly in summer. With a coverage area of 162000 km^2, the diversities of topographies also affect on precipitation changes. The topography varies from high mountains of Luoxiao, Wuyi, and Nanling in east, south and west, with the elevation reaching to the 2200m, to the depressing of Ji Tai or Ganzhou Depressing in the south or center and alluvial plains of Poyang Lake Plain in the north, with the elevation reaching to <50 m (Fig. 1a). The different topography and location generate the uneven distribution rain in space, with less rain in the depressing, plains, and hills area for the leeward sloop, but more orographic rain in the mountain area because of windward sloop (Fig. 1b) (Mingjin et al. 2011). To analyse precipitation changes in the rich- or poor-rain area, the metrological stations were classified into dry and wet stations (Fig. 1a and b), according to the annual precipitation amount. We sorted the annual precipitation averaged over the time from 1961 to 2005, of the 15 stations. The 4 stations with the max or min mean annual precipitations are set as dry or wet stations, indicating the dry or wet area, respectively.

In the past 50 years, annual mean temperature indeed experiences a significant ($p<0.02$) increase with a change rate of 0.15℃/10a (Fig.1d), based on the metrological observations from 1961 to 2005. Under the temperature increasing, the precipitation in temporal and spatial distribution becomes more uneven (Zhan et al. 2011), which increases the risk of floods and droughts (Li et al. 2016; Ye et al. 2011).

2.2 Data sets

Global Climate Models (GCMs) are widely used tools to project future climate change. GCMs from the Coupled Model Intercomparison Project Phase Five (CMIP5) performs better than other CMIPs such as CMIP3 and CMIP4, with generally finer resolution and more improved physical mechanism (Sperber, 2013; Taylor et al. 2012). Compared to the other CGMs of CMIP5, the MRI-CGCM3 (Meteorological Research Institute Coupled Ocean-Atmosphere General Circulation Model3, Yukimoto et al. 2012) performs better in simulating diurnal rainfall over subtropical China (Yuan et al. 2013) and has the finest resolution of 1.121° × 1.125°, thus being applied in Poyang Lake Watershed. From MRI-CGCM3, we select historical (1961 to 2005), historical extent (2006 to 2012) and future (2006 to 2100) precipitation and temperature simulations. The future data includes simulations of the Representative Concentration Pathways (RCPs) of 8.5,6, 4.5 and 2.6. Compared to the

other RCPs, in the RCP8.5 scenario temperature increases the most, which is corresponds to a highest greenhouse gas emission, leading to a radiative forcing of 8.5 W/m^2 and temperature increase of 7.14 °C at the end of 21st century (Taylor et al. 2012). Thus, to detect more sensitive precipitation change under climate warming, we selected future simulations in the RCP8.5 scenario.

The local grid observations (Zhao et al., 2014) with a resolution of 0.5°×0.5° are downloaded from the China Meteorological Data Service Center (http://data.cma.cn/). The local grid observations and MRI-CGCM3 historical simulations were used to construct relationship to correct the MRI-CGCM3 data. China metrology point data were also downscaled and used to validate the bias-corrected MRI-CGCM3 simulations. To investigate the relationship between precipitation changes and the temperature increase, we extract not only temperature data, but also precipitations.

To quantitatively analyse the precipitation changes under climate warming in 21st century, we compared precipitation between the baseline and future period. As annual precipitation observations have main oscillation periods of quasi-20 years (Zhan et al. 2011), we selected three 20 years, the baseline period from 1998 to 2017, the near future period from 2041 to 2060 and the far future period from 2081 to 2100. We merge historical simulations from 1998 to 2005, and historical extent simulations from 2006 to 2012, and RCP8.5 simulations from 2013 to 2017, which is the nearest 20 years and thus selected as the baseline period. The data in near and far future period are derived from simulations in RCP8.5 scenarios.

3 Methodology

3.1 Future climates projection based on the spatiotemporally distributed downscaling model

Considering the spatiotemporal heterogeneity of precipitations in the regional scale as Poyang Lake Watershed, we developed a spatiotemporally distributed downscaling model (STDDM), which is a logical framework based on a specific mathematic algorithm. The mathematic algorithm was used to create mapping relationship between GCMs simulations in the global scale and climates variables in the local scale. The mapping relationship is used as a translation function to translate future climate simulations from the GCMs scale to regional scale. In the framework, respective mapping relationships between the corresponding matche-ups of GCMs simulations and local climate observations in each different time (eg. Months or seasons)

143 at each different location, were constructed. The STDDM was improved in adjusting the specific downscaling algorithm
144 suitable to distributed space and time, where downscaling process shows spatiotemporally different in parameters or equations
145 and the output data are spatial continued, compared to the traditional downscaling methods, which ignores the temporal and
146 continuously spatial difference in the downscaling process and expresses the space by discrete points instead of continual space
147 and.
148 Figure 2a shows the logical framework of the STDDM while Fig. 2b demonstrates how it was applied in Poyang Lake
149 Watershed using MRI-CGCM3 based on a linear-scaling algorithm. The STDDM contains three parts (Fig. 2a and b): (1) Up-
150 sampling GCMs simulations and local-scale observations to a continual grid space of the same finer resolution; (2)
151 Constructing respective mapping relationship between the GCMs simulations and local observations in distributed space-time;
152 (3) Correcting the GCMs simulations of the future scenario, using the relations constructed in step 2.

153 **3.1.1 Up-sampling GCMs simulations**

154 With a coarse resolution, unable to be integrated with sub-grid scale features (Grotch and Maccracken,1991) such as
155 topography and land use, the GCMs simulations should be up-sampled to a finer resolution. To get corresponding match-ups
156 of the global-scale simulation and local-scale observation in respective time and space, we up-sampled both GCMs simulations
157 and observations into the same spatial continual grid with a high resolution (Fig. 2a).
158 In the study, MRI-GCM3 simulations were interpolated by Natural Neighbour Interpolation (Sibson et al., 1981), to a scale of
159 20 km×20 km, the smallest size of the sub-basin of Poyang Lake Watershed (Zhang et al. 2017), generating 263 spatial grids
160 (Fig. 2b). For the spatiotemporally distributed downscaling, we used China meteorology spatially continua grids as
161 observations, instead of China meteorology stations. The gridded observations were interpolated to 20 km × 20 km, the same
162 as the downscaled climate simulations. The match-up grids of simulations and observations at each time and each grid-box are
163 generated.

Hydrol. Earth Syst. Sci. Discuss., https://doi.org/10.5194/hess-2018-286
Manuscript under review for journal Hydrol. Earth Syst. Sci.
Discussion started: 12 July 2018

3.1.2 Constructing relations between the GCMs simulations and local observations

As there is an inevitable mismatch between the simulations and observations of different time and space (Li, 2009; Wood et al., 2004) after the up-sampling, bias correction should be performed. The bias correction was processed by using the translation function between match-ups of the up-sampled simulation and observation, which is the relations of the match-ups. As the influencing factors on climates show heterogeneity in space and time, we created spatiotemporal distributed relations, described by the following formula.

$$C'_{T,S} = F_{T,S}(C_{T,S}) \quad (1)$$

Where, $C'_{T,S}$ and $C_{T,S}$ indicate the up-sampled global-scale climate simulations and local climate variables respectively, in the given time of *T* and space of *S*. $F_{T,S}$ demonstrates a translation function, used to correct the up-sampled GCMs simulations. The function is a specific downscaling algorithm spatiotemporally distributed in mathematic equations or parameters, which is constructed based on the data in historical time from 1961 to 2005.

In the study, we created translation function based on a linear-scaling algorithm (Lenderink et al., 2007). For the linear-scaling algorithm, the simulations were corrected by the discrepancy between the simulations and observations in historical time. Precipitations derived from GCMs were corrected by multiplying the precipitation bias coefficient, which is the ratio of the mean monthly observation to simulation in historical time; while temperatures were corrected by adding the temperature bias coefficient, which is the difference value between mean monthly observation and simulation in control time. However, as the bias varies among the Months from January to December and locations of 236 spatial grids, the global standard bias coefficient is prohibited. To better capture the bias in distributed time and space, we should create individual bias coefficient for the given Month and gird box. Thus, a spatiotemporal distributed bias matrix was constructed. The respective downscaling model and bias coefficient for a given Month (*T*) and space (*S*) was established by Eq. 2 and 3.

$$P' = P \times P\_Cof \quad (2)$$

$$TM' = TM + TM\_Cof \quad (3)$$

where, *P* (*T*) represents the precipitation (or temperature) of up-sampled simulations. *P'* (*TM'*) represents the downscaled result or up-sampled observations; *P_Cof* (*TM_Cof*) represents the bias correction coefficient of precipitations (or

185 temperatures). In the construction of *P_Cof* (*TM_Cof*), *P* (*TM*) and *P'* (*TM'*) was set as the average monthly precipitation (or
186 temperature) over the historical time from 1961 to 2005. All the input and output data in the equations is in the given Month
187 (*T*) and space (*S*).

188 **3.1.3 Correcting the GCMs simulations**

189 The constructed relationship between the GCMs simulations and observations in historical time (in section 3.1.2), are also hold
190 for data in the future (Maraun et al., 2010). Thus, the translation function was used to correct the CGCMs simulations in the
191 future. In the study, we corrected daily and monthly precipitations (or temperatures) from MRI-CGCM3, by adding (or
192 multiplying) the bias coefficients in the corresponding Month and grid box.

193 **3.2 Precipitation changes analysis**

194 **3.2.1 Statistic indices of precipitation changes**

195 To obtain the general change in temporal distribution, we calculated monthly precipitations from 1998 to 2100, averaged over
196 the whole watershed. As flood and drought occur more frequently in wet and dry months, we specially analyze the extreme
197 wet and dry precipitation changes in the 21st century. Therein, monthly precipitations, > 75% percentile of the 12 monthly
198 precipitations, were classified as the extreme wet monthly precipitations for each year of the 103 years; monthly precipitations,
199 ≤ 25% percentile were classified as the extreme dry monthly precipitation. The monthly precipitation of 25%-50% and 50%-
200 75% quantiles are classified as normal dry and wet monthly precipitations. The wet monthly precipitations include extreme
201 and normal wet monthly precipitations while the dry monthly precipitations include extreme and normal dry monthly
202 precipitations. To further understand precipitation dynamics in frequency and intensities, daily precipitations were categorized
203 into five classes based on the classification by Chinese Meteorological Administration and the possible risk to flood-drought:
204 light rain, median rain, heavy rain, rainstorm, and extreme rainstorm with daily precipitation in 0.1-10, 10-25, 25-50, 50-100
205 and >100 mm/day, respectively. The frequency of precipitation intensities indicates heterogeneity in temporal distribution.
206 The higher frequency of moderate rain means the more homogeneous, vice versa is the extreme rain. Therefore, the
207 precipitation intensities were separated to moderate or extreme rains, including light rain, median rain or heavy rain, rainstorm,

extreme rainstorm, respectively. To analysis the changes in precipitation frequencies and intensities, we calculate the annual days of light rain, medium rain, heavy rain, rainstorm and extreme rainstorm from 1998 to 2100 averaged over the whole watershed. Annual total precipitation, annual dry days, annual max daily precipitation and annual max continual dry days are displayed as well. The all above precipitation indexes of one year for the whole watershed were calculated based on the precipitation averaged over the grids containing the 15 stations, instead of the entire grids, as the 15 metrological stations (Fig. 1a) are uniformly distributed in the whole watershed, covering all kinds of the topographies and land covers.

Under global climate warming, precipitation becomes more centred which leads to more heterogeneity in temporal and spatial distribution (Donat et al., 2016; Min et al., 2011). Thus, we calculated variation coefficients (VC) for each year from 1998 to 2100, to investigate the precipitation changes in temporal and spatial distribution. The VC is defined by the ratio of the standard deviation and average value, described by Eq. 4.

$$VC = \frac{\sqrt{\frac{\sum (x-\mu)^2}{n-1}}}{\mu} \quad (4)$$

Where, x represents monthly (or daily) precipitation of one year; n is month number (or day number) of a year and μ indicates averaged monthly or daily precipitation of a year. VC measures the standard dispersion of data items, which can indicate the unevenness of precipitations in temporal and spatial distribution. In the study, heterogeneity in temporal, spatial and spatiotemporal distribution was measured by temporal, spatial and spatiotemporal VC, respectively. Temporal VC was calculated on the daily or monthly precipitations in one year, where the VC for one year is averaged over that of the 15 stations. For monthly precipitation, we only select extreme wet and dry precipitations, as the extreme wet and dry are more likely to cause floods or droughts and thus should be pay more attractions to. Spatial VC were calculated on annual total precipitations of the 15 stations in one year. Spatiotemporal VC was calculated on the monthly precipitations of the extreme wet months of the wet stations and the extreme dry months of the dry stations in one year, as the extreme precipitation value was more likely to cause floods or droughts.

229 **3.2.2 Relationship analysis between precipitation changes and temperature increasing**

230 We investigated the precipitation changes as a result of global temperature increase. To this end, we made liner regression
231 between the precipitation index and temperature changes from 2005 to 2100. We note that a mean filter with a widow size of
232 21 years can reduce potential random fluctuation from precipitation by the most; thus was used to smooth annual precipitation
233 indexes and temperature simulations from 2005 to 2100. The long-time smoothed annual precipitation or temperature minus
234 the average annual value from 1998 to 2017, are set as precipitation index or temperature changes. A linear regression model
235 was used to investigate whether precipitation changes are related to climate warming. The two 11 years, 2005 to 2015 and
236 2090 to 2100 at the start and end, did not have filter diameter of 21 years; thus climate data used to be regressed is from 2016
237 to 2089.

238 **4 Result and Discussion**

239 **4.1 Validations of precipitation and temperature projections in Poyang Lake Watershed**

240 Before being used in future climate projection, the model was examined. Data from 1961 to 1985 were used to construct the
241 model, and the remaining historical data from 1986 to 2005 were used to validate. The determination coefficient (R^2), root
242 mean square error (RMSE) and PBias (percent bias) were used to examine the model performance.
243 To test whether the downscaling method is effective in climate projections, we compare the results before and after the bias
244 correction in Fig. 3. The projections with bias corrections show better performance with high correlations and narrow bias,
245 compared to the result without bias corrections. Considering the complexity of climate physical mechanism, which is difficult
246 to accurately simulated by the present methods, the uncertainty could be acceptable.

247 **4.2 Temporal variation of future precipitation**

248 **4.1.1 Monthly scale**

249 To facilitate discovering the general intra- and inter-annual variability over the future climate warming, we analysed the
250 monthly precipitation changes during the period from 1998 to 2100 in Fig. 4. Precipitation gathered in spring (March to May)

and summer (July to August), occupying 73% of the annual amount, which highlights the significant intra-annual dynamics of rains. Rich rain months, indicated by reddish color, are mainly in April to July (the wet season); while the poor rain months indicated by bluish color, are mainly in September to next February (the dry season). The intra-annual dynamics of precipitations is similar to that of the Feng's (2012). In the inter-annual precipitation pattern, the rich rain months become richer, and the rich rain season comes earlier from April to March, even February. Precipitations of seven months took increasing trends, of which 71% (5 out of the 7 months) are in the wet season; while precipitations of the other five months experienced decreasing trends and all the months were in the dry season.

The monsoon is the dominant factor to inter or intra annual variability of precipitation. The reaching time of the monsoon reaching Poyang Lake Watershed, varies in different years, with 1~2 months' advance or delay. Therefore, the rich or poor rain months for different years are not the same. To better demonstrate the opposite variations (the decreases in the dry period and increases in wet), monthly precipitations in each year were sorted in the descending order in Fig. 4(b). Wet monthly precipitations experienced increasing trend respectively, even with some significant sign; whereas each dry monthly precipitation exhibited decreasing trends, separately, despite the insignificant signs. We accumulated the extreme wet or dry monthly precipitations for each year in Fig. 5. The precipitation of extreme wet months showed a significantly increasing trend ($p<0.05$) (Fig. 5a), and increased from 277.82 mm•month^{-1}/a over historical time from 1998-2017, to 344.10 mm•month^{-1}/a over future time from 2081 to 2100, by 23.86 % with change rate of 7.3 mm•month^{-1}/10a; while the precipitation of extreme dry months demonstrated a significantly decreasing trend ($p<0.05$) (Fig. 5b) and decreased from 35.44 mm•month^{-1}/a over historical time from 1998-2017, to 30.46 mm•month^{-1}/a over future time from 2081 to 2100, by -14.05 % with change rate of 0.92 mm•month^{-1}/10a. Therein, the extreme wet months are mainly concentrated in March-July (Fig. 5c), part of wet season; while the extreme dry months are mainly concentrated in September-February (Fig. 5d), consistent to the dry season.

Overall, with climate warming over the 21 century, the wet monthly precipitations become wetter while the dry month precipitations become dryer, which highlights the uneven temporal distribution of precipitation (Fig. 6). As shown in Fig. 6, the temporal variation coefficient of the extreme month (including extreme wet and months) precipitations within each year from 1988 to 2100, experiences significantly increasing trends ($p<0.01$), and increased from 0.76/a over historical time from 1998-2017, to 0.84/a over future time from 2081 to 2100, by 10.53% with change rate of 0.01/10a. The significantly increasing

trends indicated the more uneven trend of precipitation in the temporal distribution, which might lead to increasing risks of floods and droughts.

4.1.2 Daily scale

To understand the changes of precipitation intensities and frequencies under the future climate warming, daily precipitation variations were also analysed in Fig. 7. Averaged over 103 years, annual precipitation frequencies are dominated by the moderate rain, a total of 163.70 days, 44.8 % (163.70/365) while the extreme rain occurs less often, a total of 20.70 days, 6.70 % (20.7/365). The remaining is rain-free days, a total of 180.75 days, 49.5% (180.75/365). Over the climate warming, the annual frequency of moderate rains experienced decreasing trends; in contrast, the annual frequency of extreme rains experienced significantly increasing trends (Fig. 7a). Statistically, the annual moderate rain frequency was decreased from 170.56 days/a over historical time from1998 to 2017, to 159.55 days/a over future time from 2081 to 2100, by -6.46% with a change rate of -14.4 days/10a; while the annual extreme rain frequency was increased from 19.18 days/a over historical time from1998 to 2017, to 23.42 days/a over future time from 2081 to 2100, by 22.10 % with a change rate of 0.49 days/10a (Fig. 7b).

The annual total rainy days, sum of moderate and extreme rains, demonstrated a significantly decreasing trends in the 21st century; whereas the annual total precipitation exhibited a significantly increasing trend (Fig, 7c). Rainy days were decreased from 187.57 days/a over historical time from1998 to 2017, to 180.37 days/a over future time from 2081 to 2100, by -3.84% with a change rate of -1.00 days/10a; while annual total rain amount was increased from 1650 mm/a over historical time from 1998 to 2017, to 1906 mm/a over future time from 2081 to 2100, by 15.55 % with a change rate of 23.00mm/10a. The increasing annual total rain and decreasing annual rainy days suggested more concentrated precipitation and dry days. The tendency might lead to increasing risk of flood-drought, which was also documented by the increasing annual max daily precipitation and max continuous dry days (Fig. 7d). Annual max daily precipitation was increased from 148.76 $mm \cdot day^{-1}/a$ averaged over historical time from1998 to 2017, to 212.01 $mm \cdot day^{-1}/a$ averaged over future time from 2081 to 2100, by 42.51% with a change rate of 7.2 $mm \cdot day^{-1}/10a$; while the max continuous dry days was increased from 25.35 days/a over historical time from 1998 to 2017, to 28.15 days/a over future time from 2081 to 2100, by 11.05% with a change rate of 0.5 days/10a.

299 Overall, the significantly inverse change tends in moderate vs extreme rain frequencies, annual total rain vs annual total rainy
300 days, and annual max precipitation vs annual max continuous rainy days, indicated an increasing temporal heterogeneity in
301 precipitation distribution over the 21st century. Obviously, the increasing heterogeneity was also exhibited by the increasing
302 temporal VC of daily precipitations (Fig. 8). The temporal VC of daily precipitation was increased from 1.50/a over historical
303 time from1998 to 2017, to 1.62 /a over future time from 2081 to 2100, by 7.48% with a change rate of 0.016/10a.

304 **4.3 Spatial variation of future precipitation**

305 Climate warming could cause the rain belt shift (Putnam et al., 2017), which might lead to precipitation changes in the spatial
306 pattern. The spatial variation was analyzed in Fig. 9 and 10. As floods and droughts occur more frequently in extreme months,
307 the precipitation in the analysis considered only the extreme wet (April-July) and dry (September-February) months (Fig. 5c
308 and d). Besides, precipitation is dominated by southeast summer monsoon, which bring water vapour from the sea. The summer
309 monsoon is frequent from the end of spring and stat of autumn, covering the wet months April to July. However, though as
310 dry months, the autumn period from September to November is affected by southeast summer monsoon (Tan et al., 1994)
311 slightly because autumns are the transpiration periods of summer to winter. Therefore, winter (December-February) was
312 represented as the dry season with poor rain; while April-July was represented as the wet season with rich rain. To visualize
313 the spatial pattern of the precipitation changes in the wet and dry season under future climate warming, we calculated the mean
314 wet or dry precipitation averaged over the historical period from 1998 to 2017 (Fig. 9a or d), the near future period from 2041
315 to 2060 (Fig. 9b or e), and the further future period from 2081 to 2100 (Fig. 9c or f), respectively. The change rate of wet or
316 dry season precipitation from 1998 to 2100 (Fig. 9g or h) were also exhibited the climate warming impacts on the spatial
317 pattern of precipitation changes.
318 As shown in Fig. 9a-c and e-g, precipitations showed a regular spatial pattern both in the wet and dry season. More specifically,
319 precipitations were distributed more in the east and west, which are dominated by southeast and southwest summer monsoon.
320 Whereas, precipitations were distributed less in the north central plain for reasons of being as the leeward sloop of the east
321 (Xuefeng Mountain) and west mountain (Wuyi Mountain), and south bottom depression due to that the water vapor was
322 blocked by the NanLing Mountain in the south (Fig. 1a). The precipitation distribution in spatial pattern from 1998 to 2100

(Fig. 9 a-c and d-f) were consistent to the observations from 1951 to 2005 (Fig. 1b.), thus confirming the satisfactory performance of the STDDM.

Yet, wet and dry season precipitations showed inverse changes. The inverse is consistent with the inter-annual variability of increasing precipitation trend in wet months and decreasing trend in dry months (Section 4.2). The wet or dry season precipitations exhibited ascending (Fig. 9a-c and g) or descending (Fig. 9d-f and h) change from 1998 to 2100, respectively. Specifically, the wet season precipitation was increased from 172.5-266.3 mm•month^{-1}/a averaged over the historical time (1998-2005), 189.9-265.3mm•month^{-1}/a averaged over the near future (2041-2060), to 219.9-345.8mm•month^{-1}/a averaged over the further future (2081-2100), with an increasing change of 3.5-11.7mm•month-1/10a, range in the cells of the whole watershed (Fig. 9 a-c, g). In contrast, the dry season precipitation was decreased from 68.4-99.9mm•month^{-1}/a averaged over the historical time (1998-2005), 66.5-99.0 mm•month^{-1}/a averaged over the near future (2041-2060), to 56.7-84.9 mm•month^{-1}/a averaged over the further future (2081-2100), with an decreasing change of -2.7- -1.1mm•month^{-1}/10a, range in the cells of the entire watershed (Fig. 9 d-f, h). The tendency of being wetter in wet seasons and drier in dry seasons might lead to increasing risks of floods and droughts.

The increase of precipitation in wet seasons or decrease in dry seasons were also detected in the cells over the entire watershed (Fig. 9g or h). However, the spatial patterns of changes are complex with regionally different signs (Fig. 9g and h). The wet season precipitation increase was different in spatial distribution, with change rate raising from ≤3.6 mm/10a in the southwest, to ≥11.7 mm/10a in northeast; while the decrease of the dry season precipitation in falls from ≥ -2.0 mm/10a in the surroundings, to ≤ -2.7 mm/10a in the centre. In the wet season, the precipitation increased more in the north part of the watershed except for the centre plain (Fig. 9g); while in the dry season the precipitation decreased more in the center area (Fig. 9h). The uneven change rates indicated the increasing heterogeneity of precipitations in the spatial distribution (Fig. 10a). Specifically, the heterogeneity was raised with the spatial VC increasing from 0.097/a over historical time from1998 to 2017, to 0.110/a over future time from 2081 to 2100, by 12.64% with a change rate of 0.002/10a.

However, precipitation changes show a different spatial pattern between wet and dry seasons. From 1998 to 2100, in the wet season (Fig 9a-c), the wet area (the reddish area, mainly in the north except for the center plain) become wetter; while in the dry season (Fig. 9 d-f), the dry area (the bluish area, mainly in the north center plain and south depression) become drier. The

348 tendency of being wetter in the wet area and drier in the dry area might enhance the risk of floods and droughts. The drier
349 condition in the dry season and area and wetter condition in the wet season and area also indicated the increasing heterogeneity
350 of precipitations in the spatiotemporal distribution (Fig. 10b). Specifically, the heterogeneity was raised with the
351 spatiotemporal VC increasing from 0.89/a over historical time from1998 to 2017, to 0.94 /a over future time from 2081 to
352 2100, by 4.96% with a change rate of 0.008/10a.

353 **4.4 The impact assessment of temperature increasing on precipitation changes**

354 Previous studies have detected precipitation changes, and attribute these to climate warming (Westra et al., 2013; Zhang et al.,
355 2013). In the study, the spatiotemporal changes of precipitation in Poyang Lake Watershed in the 21st century were supposed
356 to be related to the increasing temperature.
357 The following are trying to demonstrate the driving force related climate warming on precipitation changes in the temporal
358 pattern. In the wet season from April to July, the summer monsoon might becomes weaker in the southeast of Asia, with the
359 climate warming (Wang, 2001; Wang, 2002; Guo et al., 2003). Consequently, summer monsoon delays in the middle and
360 lower Yangtze River basin for a longer time, instead of moving further north. The delays lead to much more rain during the
361 wet season. Located in the middle Yangtze River basin, Poyang Lake Watershed becomes wetter in the wet season (Fig. 4-5,
362 Fig. 9a-c). In fact, the increase of precipitation in Poyang Lake Watershed was detected in previous studies (Yu and Zhou,
363 2007; Ding et al., 2008). In the poor-rain period from September to next February (especially winter time from December to
364 February) with low-frequency summer monsoon, there is less water vapor in atmospheres, which is not easy to condense into
365 rain. Additionally, stronger winds in winter (Wu et al., 2013) blow the evaporation away. The stronger wind in winter enhances
366 the difficulty to gather enough water vapor to rain, compared to the other seasons. When temperature increases over the 21st
367 century, the atmospheres ability of holding water vapors is strengthened, which make it more difficult to precipitate. Therefore,
368 precipitations decrease in the dry season, similar to Li et al.'s (2016) research. As climate warming increases the ability of
369 atmosphere to contain water vapor, it is harder to condense into rain only if it has enough more water vapor (Min et al., 2011;
370 Zhang et al., 2013). Thus, the frequency of heavy rain and free-rain increases, which indicates more frequency of extreme rains
371 and less of moderate rains. Overall, climate warming might make precipitation more uneven in temporal distribution.

372 Climate warming could also explain the spatial distribution of precipitation change in dry and wet seasons. In the wet season,
373 the summer monsoon delays in middle and lower Yangtze River Basin. The delaying area covers only the north part of Poyang
374 Lake Watershed. Because of getting rich water vapor from the delayed summer monsoon, precipitation in the north part of
375 Poyang Lake Watershed are increased more with larger change rate (Fig. 9g). The east of Poyang Lake Watershed is the nearest
376 to the sea, west of Pacific Ocean; thus the east can get more water vapor continually. That's why the change rate decreases
377 from the southeast to northwest. However, in the dry season especially in winter, which is with low-frequency or even no
378 summer monsoon, the water vapor mainly comes from evapotranspiration. In the watershed, there is more evapotranspiration
379 in the periphery, which is covered by high-density vegetation in the northwest, southeast, southwest mountains, and lake of
380 Poyang in the north plain; while there is less in the center, mainly covered by farmland and grassland (Wu et al., 2013). Thus,
381 the moisture decreases from the surroundings to the center. Therefore, it is more difficult to rain in lower moisture area, the
382 center part of Poyang Lake Watershed as temperature increases; thus the precipitation decreasing rate falling from the
383 surroundings to the center in the dry season (Fig. 9h).
384 To quantitatively analyze the relationship between precipitation changes and temperature increasing, we made scatter plot
385 between precipitation indexes changes and temperature increases in Fig. 11. Trend analysis was conducted by linear regression
386 over each annual precipitation indexes against the 103 years from 1998 to 2100. The associated slopes represented the change
387 rate for each long-term precipitation indexes. The trend significant sign was indicated by p value. As shown in Fig. 11, there
388 is statically significant correlations between precipitation changes and temperature increasing, with significant sign of $p \leq$
389 0.001 and $R \geq 0.78$ for 6 precipitation indexes, annual precipitation in wet season (Fig. 11a), annual max daily precipitation
390 (Fig. 11d), temporal VC of monthly precipitation (Fig. 11c), temporal VC of daily precipitation (Fig. 11f), spatial VC (Fig.
391 11g) and spatiotemporal VC (Fig. 11h). However, the change of the other two precipitation indexes, annual precipitation in
392 the dry season (Fig. 11b) and annual max continual dry days (Fig. 11e), appeared correlated with slight signs of $p \leq 0.05$ and
393 $R \leq 0.58$. The overestimation of light or free-rain from GCM simulations (Teutschbein et al. 2012) might explains the slight
394 correlations for annual precipitation in the dry season; while the overestimation of precipitation frequencies (Prudhomme et
395 al. 2003) could be the reason of the slight correlation for annual max continual dry days. For all the correlations (Fig. 11a-h),
396 precipitation changed with fluctuation, which might be caused by random variations of GCMs.

Despite the slight signs and stochastic fluctuation, the correlations exhibited that climate warming can partly explained the precipitation changes, with variations of 16.657 mm•month^{-1}/K, -4.31 mm•month^{-1} /K, 17.45 mm•day^{-1} /K, 0.71 days/K, 0.028/K, 0.033/K, 0.0074/K and 0.02/K for annual precipitation in the wet season, annual precipitation in the dry season, annual max daily precipitation, annual max continual dry days, temporal VC of monthly precipitation, and temporal VC daily precipitation, spatial VC and spatiotemporal VC, respectively.

5 Conclusion

A spatiotemporal distributed downscaling method (STDDM) was proposed. The downscaling method considered the heterogeneity in spatial and temporal distributions, and produced local climate variables as spatial continuous data instead of independent and discrete points. The spatially continuous future precipitation distribution and dynamics in the wet and dry season are constructed and several findings are obtained.

Firstly, the heterogeneity of precipitation in the spatial and temporal pattern is enhanced under future climate warming. In the temporal pattern, the wet season precipitation increased with change rate of 7.33 mm/10a and 11.66 mm/K; while the dry season precipitation decreased with change rate of -0.92 mm/10a and -4.31 mm/K. The extreme precipitation frequency and intensity were strengthened with change rate of 0.49 days/10a and 7.2mm•day^{-1}/a. The inverse changes in the dry and wet season, and the increasing extremes frequencies demonstrated an ascending heterogeneity of precipitation in temporal distribution, with the change rate of 0.01/10a (0.028/K) or 0.016/10a (0.033/K) for temporal VC of monthly or daily precipitation. In the spatial pattern, the uneven change rates of the entire cells covering the watershed demonstrated an increasing heterogeneity in spatial distribution, with the change rate of 0.002/10a (0.0074/K) for the spatial VC. In the spatiotemporal pattern, the wet areas become wetter in the wet season and the dry areas become drier in dry season, which manifested an increasing heterogeneity in the spatiotemporal distribution and the change rate was 0.002/10a (0.02/K) respectively.

Secondly, analysis with temperature increases showed that precipitation changes in the spatial and temporal pattern appear to be significantly related to the climate warming. Precipitation changes can be significantly explained by temperature increasing with $p < 0.05$ and $R \geqslant 0.56$. The variability of annual precipitation in the wet season, annual precipitation in the dry season,

annual max daily precipitation, annual max continual dry days, temporal VC of monthly precipitation, and temporal VC of daily precipitation, spatial VC and spatiotemporal VC, are 16.657 mm/K, -4.31 mm/K, 0.028/K, 17.45 mm/K, 0.71 days/K, 0.033/K, 0.0074/K and 0.02/K, respectively.

This study demonstrates the precipitation changes under climate warming in the 21st century. The wetter condition in the wet season and drier condition in the dry season are expected to cause an increased risk of floods and droughts in the future. The results can be applied to a hydrological and hydrodynamic model to study the future changes of water resource, lake level and area response to climate warming. The relationship between precipitation variations and temperature increasing could be helpful to driving force analysis on rainfall changes. Furthermore, for the region where floods and droughts did not occur frequently, additional adaptation measures could be taken to prevent loss from more frequent and serious hydrological disasters.

Data availability

All data can be accessed as described in Sect. 2.2. The data sets and model codes are provided in the supplements.

Acknowledgements

This work was funded by the National Natural Science Funding of China (NSFC) (41331174, 41461080), the National Key Research and Development Program (2017YFB0504103), the Open Foundation of Jiangxi Engineering Research Center of Water Engineering Safety and Resources Efficient Utilization (OF201601), the ESA-MOST Cooperation DRAGON 4 Project (EOWAQYWET), the Fundamental Research Funds for the Central Universities (2042018kf0220) and the LIESMARS Special Research Funding.

Reference

Alexander, L. V., Zhang, X., Peterson, T. ., Caesar, J., Gleason, B., Klein Tank, A. M. G., Haylock, M. R., Collins, W. D. and Trewin, B.: Global observed changes in daily climate extremes of temperature and precipitation, J. Geophys. Res., 111, D05109, doi:10.1029/2005JD006290, 2006.

442 Baigorria, G. A. and Jones, J. W.: GiST: A Stochastic Model for Generating Spatially and Temporally Correlated Daily
443 Rainfall Data, J. Clim., 23(22), 5990–6008, doi: 10.1175/2010jcli3537.1, 2010.
444 Beven, K. J.: A Discussion of distributed hydrological modelling, Distrib. Hydrol. Model., 255–278, doi:10.1007/978-94-009-
445 0257-2_13, 1996.
446 Chen, H. and Sun, J.: How the "best" models project the future precipitation change in China, Adv. Atmos. Sci., 26(4), 773–
447 782, doi:10.1007/s00376-009-8211-7, 2009.
448 Chu, J. T., Xia, J., Xu, C. Y. and Singh, V. P.: Statistical downscaling of daily mean temperature, pan evaporation and
449 precipitation for climate change scenarios in Haihe River, China, Theor. Appl. Climatol., 99(1–2), 149–161,
450 doi:10.1007/s00704-009-0129-6, 2010.
451 Dai, A.: Increasing drought under global warming in observations and models, Nat. Clim. Chang., 3(1), 52–58,
452 doi:10.1038/nclimate1633, 2013.
453 DHI (Danish Hydraulic Institute): MIKE SHE, User Manual, Volume 1: User Guide. Hørsholm: Danish Hydraulic Institute,
454 2014.
455 Dyderski, M. K., Paź, S., Frelich, L. E. and Jagodziński, A. M.: How much does climate change threaten European forest tree
456 species distributions?, Glob. Chang. Biol., doi:10.1111/gcb.13925, 2017.
457 Engman, E. T.: Remote sensing in hydrology, Geophys. Monogr. Ser., 108, 165–177, doi:10.1029/GM108p0165, 1998.
458 Enke, W., Schneider, F. and Deutschländer, T.: A novel scheme to derive optimized circulation pattern classifications for
459 downscaling and forecast purposes, Theor. Appl. Climatol., 82(1–2), 51–63, doi:10.1007/s00704-004-0116-x, 2005.
460 Feng, L., Hu, C., Chen, X., Cai, X., Tian, L. and Gan, W.: Assessment of inundation changes of Poyang Lake using MODIS
461 observations between 2000 and 2010, Remote Sens. Environ., 121, 80–92, doi:10.1016/j.rse.2012.01.014, 2012a.
462 Feng, L., Hu, C., Chen, X., Tian, L. and Chen, L.: Human induced turbidity changes in Poyang Lake between 2000 and 2010:
463 Observations from MODIS, J. Geophys. Res. Ocean., 117(7), doi:10.1029/2011JC007864, 2012b.
464 Giorgi, F.: Simulation of Regional Climate Using a Limited Area Model Nested in a General Circulation Model, J. Clim., 3(9),
465 941–963, doi:10.1175/1520-0442(1990)003<0941:SORCUA>2.0.CO;2, 1990.

466 Giorgi, F.: Simulation of Regional Climate Using a Limited Area Model Nested in a General Circulation Model, J. Clim., 3(9),
467 941–963, doi:10.1175/1520-0442(1990)003<0941:SORCUA>2.0.CO;2, 1990.
468 Grotch, S. L. and MacCracken, M. C.: The Use of General Circulation Models to Predict Regional Climatic Change, J. Clim.,
469 4(3), 286–303, doi:10.1175/1520-0442(1991)004<0286:TUOGCM>2.0.CO;2, 1991.
470 Guo, J.L., Guo, S., Guo, J., Chen, H.: Prediction of Precipitation Change in Poyang Lake Basin. Journal of Yangtze River
471 Scientific Research Institute, 8, 007, 2010.
472 Han, X., Chen, X. and Feng, L.: Four decades of winter wetland changes in Poyang Lake based on Landsat observations
473 between 1973 and 2013, Remote Sens. Environ., 156, 426–437, doi:10.1016/j.rse.2014.10.003, 2014.
474 Hong X, Guo S, Guo J, et al. Projected changes of extreme precipitation characteristics in the Poyang Lake Basin based on
475 statistical downscaling model. Journal of Water Resources Research, 3(6), 511-521, doi:10.12677/JWRR.2014.36063, 2014.
476 Lenderink, G., Buishand, A. and Van Deursen, W.: Estimates of future discharges of the river Rhine using two scenario
477 methodologies: Direct versus delta approach, Hydrol. Earth Syst. Sci., 11(3), 1145–1159, doi:10.5194/hess-11-1145-2007,
478 2007.
479 Li, H., Sheffield, J. and Wood, E.: Bias correction of monthly precipitation and temperature fields from Intergovernmental
480 Panel on Climate Change AR4 models using equidistant quantile, J. Geophys. Res., 115(10), D10101,
481 doi:10.1029/2009JD012882, 2010.
482 Li, Y. L., Tao, H., Yao, J. and Zhang, Q.: Application of a distributed catchment model to investigate hydrological impacts of
483 climate change within Poyang Lake catchment (China), Hydrol. Res., 47(S1), 120–135, doi:10.2166/nh.2016.234, 2016.
484 Liu, C. M., Liu, W. Bin, Fu, G. Bin and Ouyang, R. L.: A discussion of some aspects of statistical downscaling in climate
485 impacts assessment, Shuikexue Jinzhan/Advances Water Sci., 23(3), 427–437, doi:CNKI: 32.1309.P.20120501.1616.002,
486 2012.
487 Lohmann, D., Rashke, E., Nijssen, B. and Lettenmaier, D. P.: Regional scale hydrology: I. Formulation of the VIC-2L model
488 coupled to a routing model, Hydrol. Sci. J., 43(1), 131–141, doi:10.1080/02626669809492107, 1998.
489 Min, Q., Min, D.: Drought Change Characteristics and Drought Protection Countermeasures for Poyanghu Lake Basin, Journal
490 of China Hydrology, 1, 84-88, 2010.

491 Min, S. K., Zhang, X., Zwiers, F. W. and Hegerl, G. C.: Human contribution to more-intense precipitation extremes, Nature,
492 470(7334), 378–381, doi:10.1038/nature09763, 2011.
493 Mullan, D., Chen, J. and Zhang, X. J.: Validation of non-stationary precipitation series for site-specific impact assessment:
494 comparison of two statistical downscaling techniques, Clim. Dyn., 46(3–4), 967–986, doi:10.1007/s00382-015-2626-x, 2016.
495 Pall, P., Aina, T., Stone, D. A., Stott, P. A., Nozawa, T., Hilberts, A. G. J., Lohmann, D. and Allen, M. R.: Anthropogenic
496 greenhouse gas contribution to flood risk in England and Wales in autumn 2000, Nature, 470(7334), 382–385,
497 doi:10.1038/nature09762, 2011.
498 Prudhomme, C., Reynard, N. and Crooks, S.: Downscaling of global climate models for flood frequency analysis: Where are
499 we now, Hydrol. Process., 16, 1137–1150, 2002.
500 Putnam, A. E. and Broecker, W. S.: Human-induced changes in the distribution of rainfall, Sci. Adv., 3(5),
501 doi:10.1126/sciadv.1600871, 2017.
502 Riahi, K., Rao, S., Krey, V., Cho, C., Chirkov, V., Fischer, G., Kindermann, G., Nakicenovic, N. and Rafaj, P.: RCP 8.5-A
503 scenario of comparatively high greenhouse gas emissions, Clim. Change, 109(1), 33–57, doi:10.1007/s10584-011-0149-y,
504 2011.
505 Segu, P. Q.: Comparison of three downscaling methods in simulating the impact of climate change on the hydrology of
506 Mediterranean basins, J. Hydrol., 383, 111–124, 2010.
507 Sibson, R: A brief description of natural neighbour interpolation. Interpreting multivariate data, 1981.
508 Sperber, K. R., Annamalai, H., Kang, I. S., Kitoh, A., Moise, A., Turner, A., Wang, B. and Zhou, T.: The Asian summer
509 monsoon: An intercomparison of CMIP5 vs. CMIP3 simulations of the late 20th century, Clim. Dyn., 41(9–10), 2711–2744,
510 doi:10.1007/s00382-012-1607-6, 2013.
511 Tan, Ruizhi: A Study on the Regional Energetics during Break, Transitional and Active Periods of the Southwest Monsoon in
512 South East Asia, SCIENTIA ATMOSPHERICA SINICA, 1994.
513 Taylor, K. E., Stouffer, R. J. and Meehl, G. A.: An overview of CMIP5 and the experiment desing. American Meteorological
514 Society, Bulletim Am. Meteorol. Soc., 93, 485–498, doi:10.1175/BAMS-D-11-00094.1, 2012.

515 Teutschbein, C. and Seibert, J.: Bias correction of regional climate model simulations for hydrological climate-change impact
516 studies: Review and evaluation of different methods, J. Hydrol., 456–457, 12–29, doi:10.1016/j.jhydrol.2012.05.052, 2012.
517 Teutschbein, C. and Seibert, J.: Is bias correction of regional climate model (RCM) simulations possible for non-stationary
518 conditions, Hydrol. Earth Syst. Sci., 17(12), 5061–5077, doi:10.5194/hess-17-5061-2013, 2013.
519 Toggweiler, J. and Key, R.: Ocean circulation: Thermohaline circulation, Encycl. Atmos. Sci., 4, 1549–1555., doi:10.1002/joc,
520 2001.
521 Trenberth K E.: Changes in precipitation with climate change, Clim. Res., 47(1–2), 123–138, 2011.
522 Wang H, Zhao G, Peng J, et al.: Precipitation characteristics over five major river systems of Poyang drainage areas in recent
523 50 years. Resources and Environment in the Yangtze Basin, 7, 615-619, 2009.
524 Wang, J., Hong, Y., Li, L., Gourley, J. J., Khan, S. I., Yilmaz, K. K., Adler, R. F., Policelli, F. S., Habib, S., Irwn, D., Limaye,
525 A. S., Korme, T. and Okello, L.: The coupled routing and excess storage (CREST) distributed hydrological model, Hydrol.
526 Sci. J., 56(1), 84–98, doi:10.1080/02626667.2010.543087, 2011.
527 Weisheimer, R. M. A. L. A. and Gutiérrez, J. M.: Can bias correction and statistical downscaling methods improve the skill of
528 seasonal precipitation forecasts ?, Clim. Dyn., 50(3), 1161–1176, doi:10.1007/s00382-017-3668-z, 2018.
529 Wilby, R. and Dawson, C. W.: SDSM 4.2-A decision support tool for the assessment of regional climate change impacts, 94,
530 2007.
531 Wilks, D. S.: Use of stochastic weather generators for precipitation downscaling, Wiley Interdiscip. Rev. Clim. Chang., 1(6),
532 898–907, doi:10.1002/wcc.85, 2010.
533 WU, G., LIU, Y., ZHAO, X., & YE, C.: Spatio-temporal variations of evapotranspiration in Poyang Lake Basin using MOD16
534 products, Geographical Research, 32(4), 617-627, 2013.
535 Wu, J., Zha, J. and Zhao, D.: Evaluating the effects of land use and cover change on the decrease of surface wind speed over
536 China in recent 30 years using a statistical downscaling method, Clim. Dyn., 48(1–2), 131–149, doi:10.1007/s00382-016-
537 3065-z, 2017.
538 Wu, Q., Nie, Q., Zhou, R.: Analysis of wind energy resources reserves and characteristics in mountain area of Jiangxi province,
539 Journal of Natural Resources, 28(9), 1605-1614, doi: 10.11849/zrzyxb.2013.09.015, 2013.

Xu, C. Y.: From GCMs to river flow: A review of downscaling methods and hydrologic modelling approaches, Prog. Phys. Geogr., 23(2), 229–249, doi:10.1191/030913399667424608, 1999.

Ye, X., Zhang, Q., Bai, L. and Hu, Q.: A modeling study of catchment discharge to Poyang Lake under future climate in China, Quat. Int., 244(2), 221–229, doi:10.1016/j.quaint.2010.07.004, 2011.

Yuan, W.: Diurnal cycles of precipitation over subtropical China in IPCC AR5 AMIP simulations, Adv. Atmos. Sci., 30(6), 1679–1694, doi:10.1007/s00376-013-2250-9, 2013.

Yukimoto, S., Adachi, Y., Hosaka, M., et al.: A New Global Climate Model of the Meteorological Research Institute: MRI-CGCM3-Model Description and Basic Performance, J. Meteorol. Soc. Japan, 90A, 23–64, doi:10.2151/jmsj.2012-A02, 2012.

Zhan, M., Yin, J. and Zhang, Y.: Analysis on characteristic of precipitation in Poyang Lake Basin from 1959 to 2008, Procedia Environ. Sci., 10, 1526–1533, doi:10.1016/j.proenv.2011.09.243, 2011.

Zhang, L., Lu, J., Chen, X., Liang, D., Fu, X., Sauvage, S. and Perez, J. M. S.: Stream flow simulation and verification in ungauged zones by coupling hydrological and hydrodynamic models: A case study of the Poyang Lake ungauged zone, Hydrol. Earth Syst. Sci., 21(11), 5847–5861, doi:10.5194/hess-21-5847-2017, 2017.

Zhang, Q., Ye, X. chun, Werner, A. D., Li, Y. liang, Yao, J., Li, X. hu and Xu, C. yu: An investigation of enhanced recessions in Poyang Lake: Comparison of Yangtze River and local catchment impacts, J. Hydrol., 517, 425–434, doi:10.1016/j.jhydrol.2014.05.051, 2014.

Zhang, X., Wan, H., Zwiers, F. W., Hegerl, G. C. and Min, S. K.: Attributing intensification of precipitation extremes to human influence, Geophys. Res. Lett., 40(19), 5252–5257, doi:10.1002/grl.51010, 2013.

Zhao, Y., Zhu, J. and Xu, Y.: Establishment and assessment of the grid precipitation datasets in China for recent 50 years, J. Meteorol. Sci., 34(4), 4–10, 2014.

Zorita, E. and Von Storch, H.: The analog method as a simple statistical downscaling technique: Comparison with more complicated methods, J. Clim., 12, 2474–2489, doi:10.1175/1520-0442(1999)012<2474:TAMAAS>2.0.CO;2, 1999.

Hydrol. Earth Syst. Sci. Discuss., https://doi.org/10.5194/hess-2018-286
Manuscript under review for journal Hydrol. Earth Syst. Sci.
Discussion started: 12 July 2018

562 **Figures**

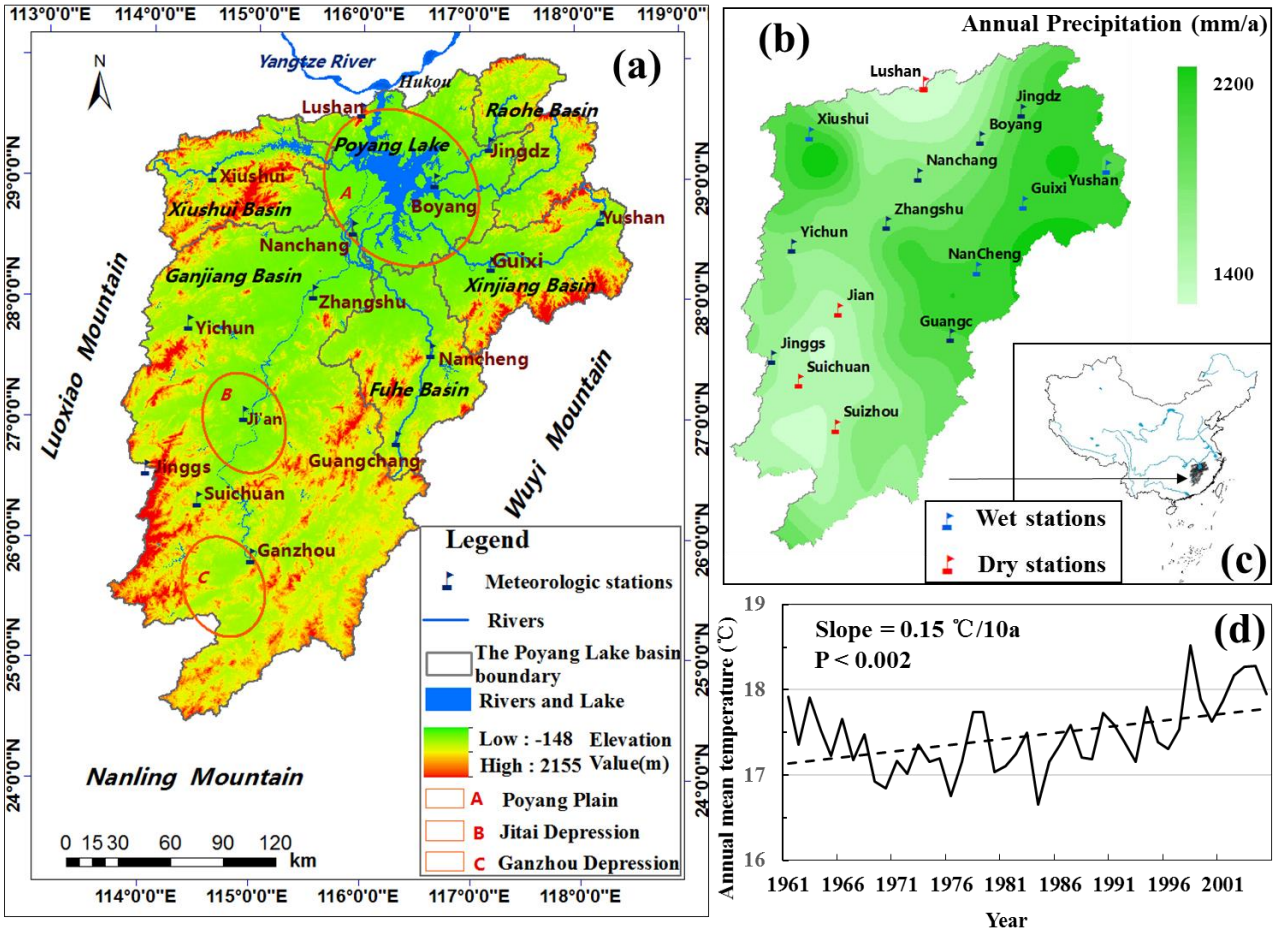

563

564 Fig. 1. The topography and landforms (a), precipitation distribution and dry-wet stations (b), temperature change (d) and
565 location of Poyang Lake Basin (c). We sorted annual total precipitations averaged over time from 1961 to 2005, of the 15
566 stations. The 4 stations with the max or min mean annual precipitations are set as dry or wet stations.

Hydrol. Earth Syst. Sci. Discuss., https://doi.org/10.5194/hess-2018-286
Manuscript under review for journal Hydrol. Earth Syst. Sci.
Discussion started: 12 July 2018

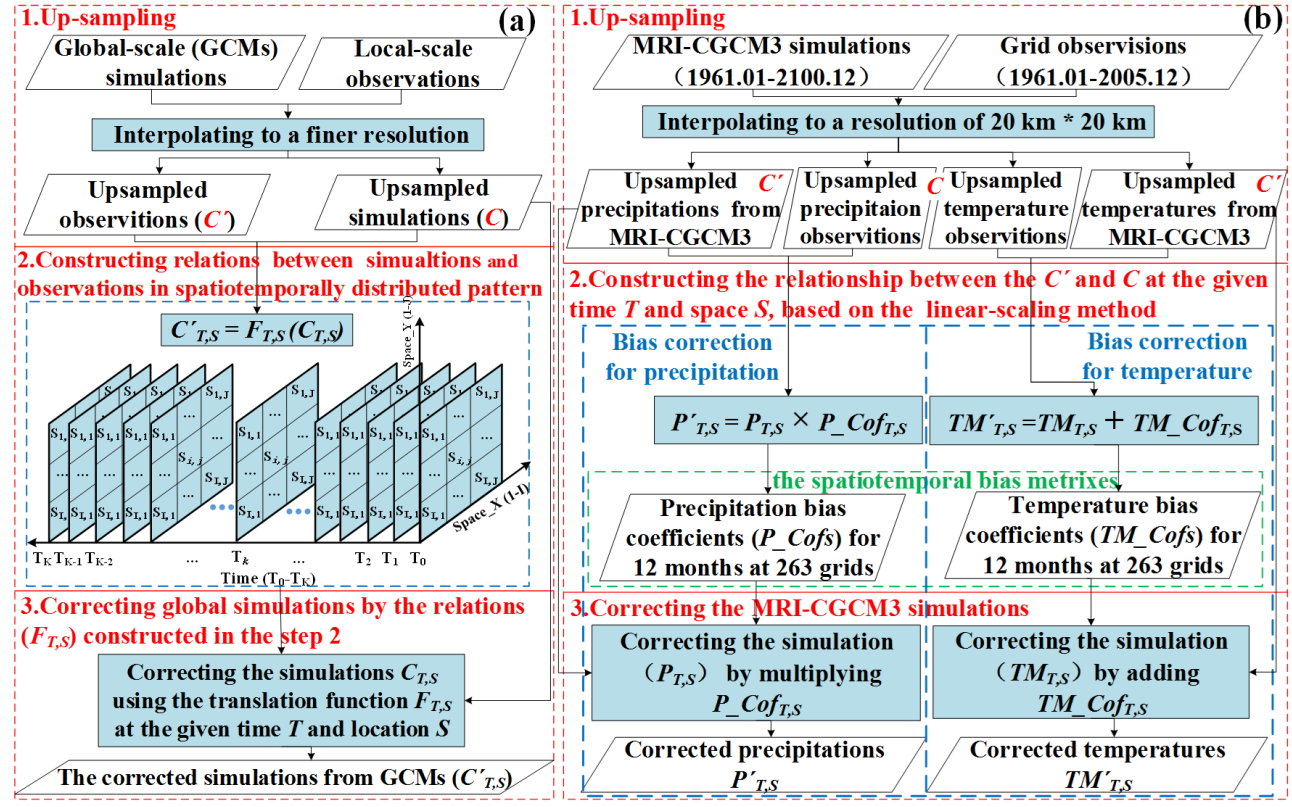

Fig. 2 Conceptual flow chart of climate projection including up-sampling, relation construction and correction: The common framework of the STDDM (a) and test case base on linear-scaling algorithm (b). The STDDM was used to projected MRI-CGCM3 simulations from 1998 to 2100.

Hydrol. Earth Syst. Sci. Discuss., https://doi.org/10.5194/hess-2018-286
Manuscript under review for journal Hydrol. Earth Syst. Sci.
Discussion started: 12 July 2018

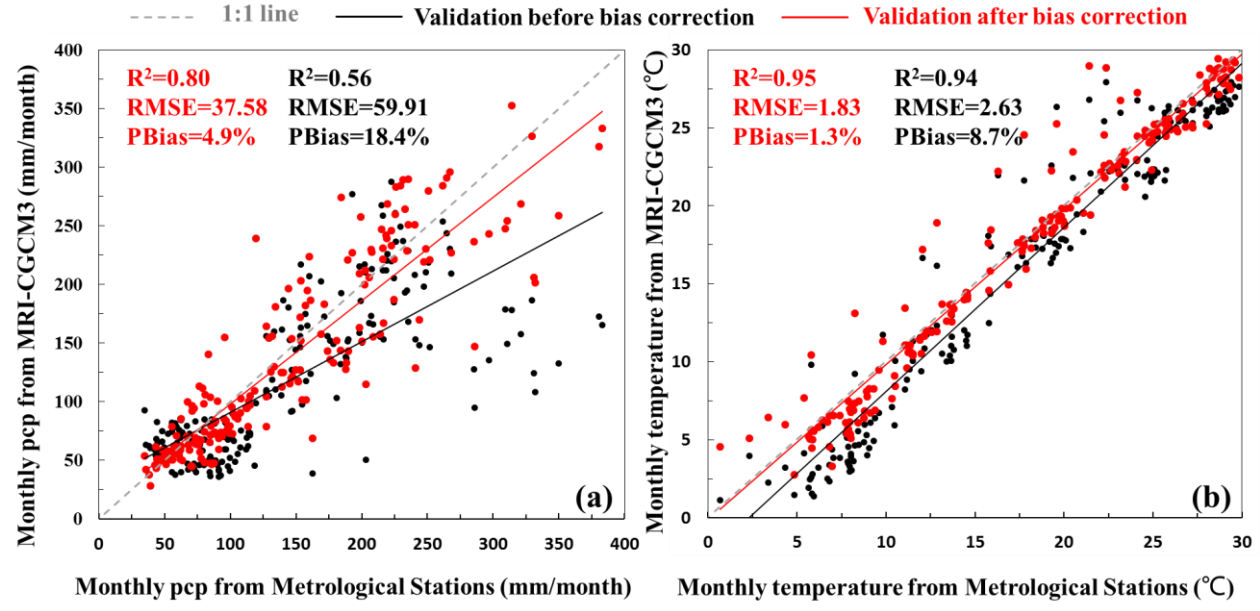

Fig. 3. Validation of precipitation (pcp) (a) and temperature (b) projection before (in black) and after (in red) bias correction. Dots represent the monthly precipitations (or temperature) from January to December, averaged over 20 years from 1986 to 2005. The dots contain monthly precipitations of the 15 stations. The solid lines represent linear regression which is best fit though all match-ups of the projections and observations.

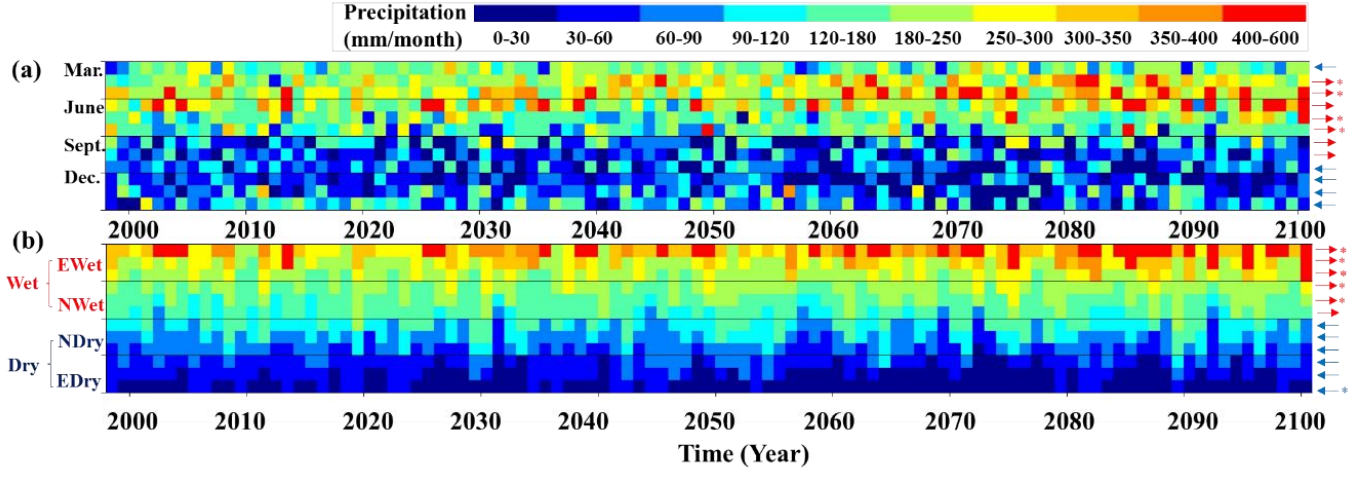

Fig. 4. Total variability of monthly precipitation from 1998 to 2100. Each column represents the data of one year and each cell represents an accumulative precipitation of one month. The red and blue arrows indicate that the monthly precipitation experienced an increasing or

Hydrol. Earth Syst. Sci. Discuss., https://doi.org/10.5194/hess-2018-286
Manuscript under review for journal Hydrol. Earth Syst. Sci.
Discussion started: 12 July 2018

Hydrology and Earth System Sciences
Discussions

579 decreasing trends over the 103 years, respectively. The asterisk demonstrates the significant trends with p<0.05. (a) Monthly precipitation
580 in month order, referred to Spring (March to May), summer (June to August), autumn (September to November), and winter (December to
581 next February) from top to bottom, respectively. (b) Monthly precipitation, sorted in the descending order for each year， where months are
582 classified as extreme wet (EWet), normal wet (NWet), normal dry (NDry) and extreme dry (Edry) months from up to down. Therein, wet
583 months (Wet) include extreme and normal wet ones while dry months (Dry) include extreme and normal dry ones.

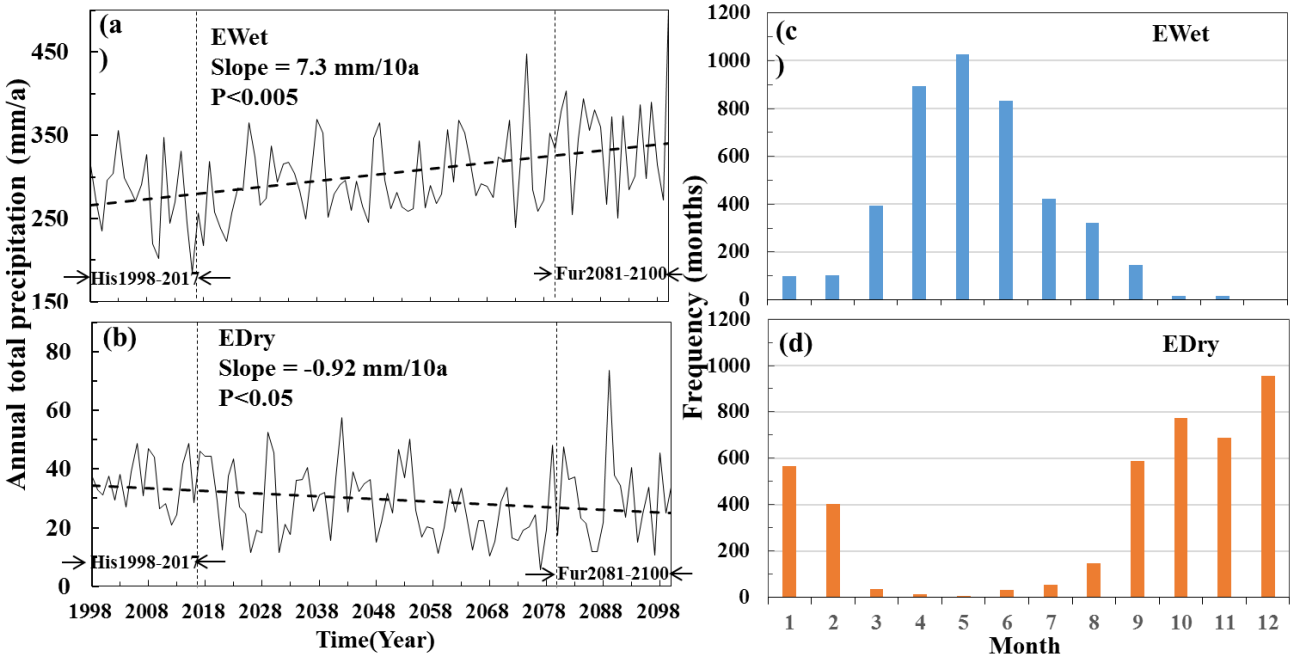

584

585 Fig. 5 The change trends of monthly precipitations of extreme wet (EWet) (a) and dry (EDry) (b) months from 1998 to 2100.
586 The far future period from 2081 to 2100 (Fur2081-2100) and baseline period from 1998 to 2017 (His1998-2017) are indicated
587 by arrows. Frequencies of the Months in extreme wet (c) or dry (d) months are calculated during the period from 1998 to 2100.

Hydrol. Earth Syst. Sci. Discuss., https://doi.org/10.5194/hess-2018-286
Manuscript under review for journal Hydrol. Earth Syst. Sci.
Discussion started: 12 July 2018

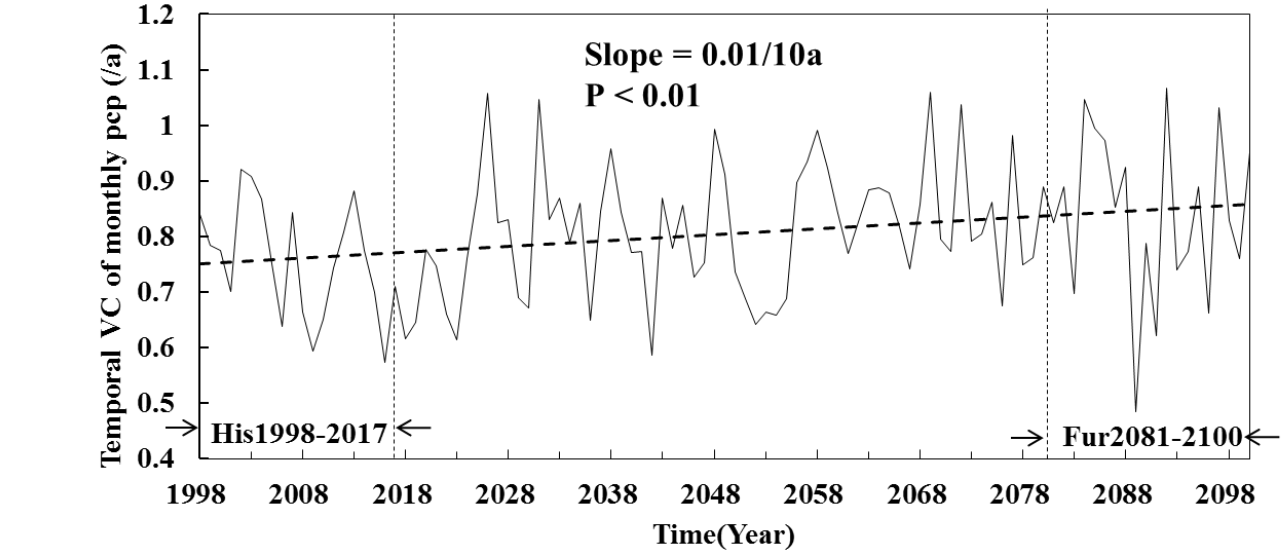

Fig. 6. The temporal variation coefficients of the extreme month precipitations for each year over 1988 to 2100. The extreme months are composed of the extreme wet and dry months. The far future period from 2081 to 2100 (Fur2081-2100) and baseline period from 1998 to 2017 (His1998-2017) are indicated by arrows.

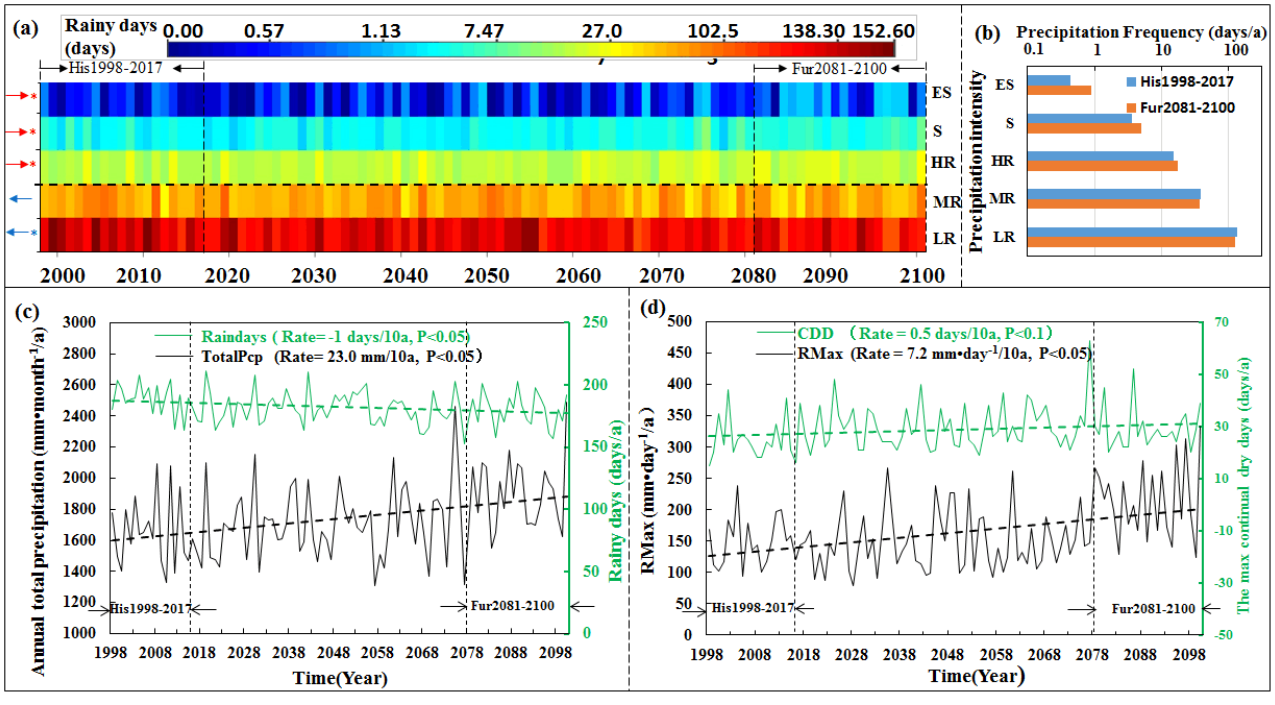

593 Fig. 7. The changes of daily precipitation intensities and frequencies. (a) Precipitation intensities and frequencies for each year
594 over 1998 to 2100, where each column represents a year and each row indicates a precipitation intensity. Daily precipitation
595 intensities are categorized to 5 classes, Light Rain (LR), Median Rain (MR), Heavy Rain (HR), Rainstorm (S), and Extreme
596 Rainstorm (ES) with daily precipitation in 0.1-10, 10-25, 25-50, 50-100 and >100 mm/day, respectively. The moderate rain
597 includes LR and MR while the extreme rain is composed of HR, S and ES. The cell represents annual frequency of one
598 precipitation intensity, with unit of days. The red or blue arrows indicate that annual frequency of the precipitation intensity
599 experienced an increasing or decreasing trends over the 103 years (from 1998 to 2100), respectively. The asterisk represents
600 the significant trends with $p<0.05$. The far future period from 2081 to 2100 (Fur2081-2100) and baseline period from 1998 to
601 2017 (His1998-2017) are indicated by arrows. (b) Precipitation frequencies of LR, MR, HR, S and ES for Fur2081-2100 and
602 His1998-2017, respectively. (c) The change of the long-term data for annual total precipitation (totalPcp) and total rainy days.
603 (d) The change of the long-term data for annual max daily precipitation (RMax) and annual max continuous dry days (CCD).

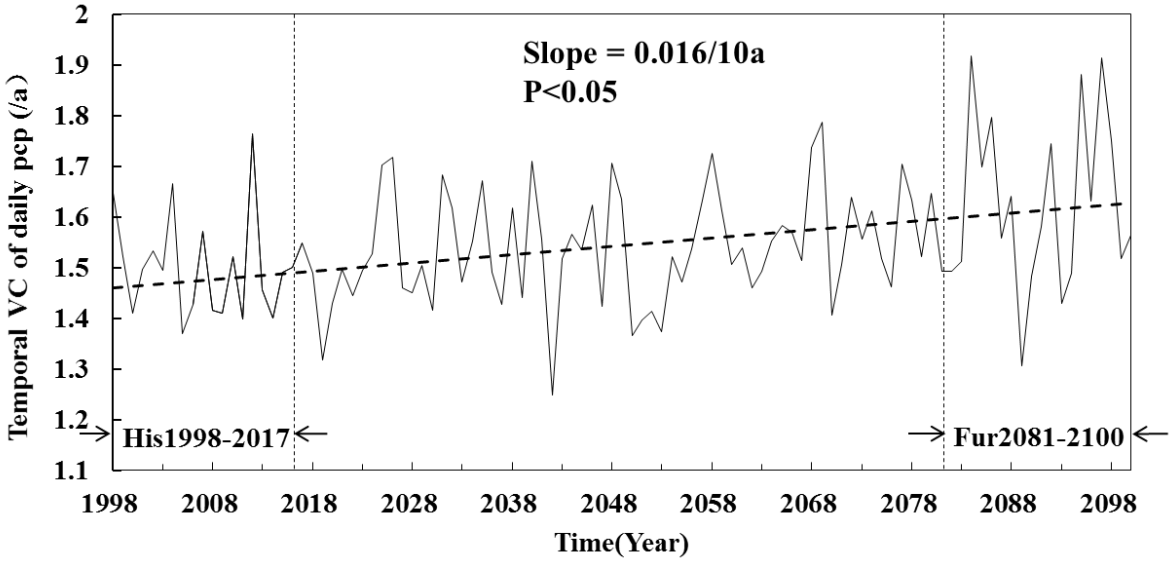

604

605 Fig. 8. The temporal variation coefficient of daily precipitations for each year over 1988 to 2100. The far future period from
606 2081 to 2100 (Fur2081-2100) and baseline period from 1998 to 2017 (His1998-2017) are indicated by arrows.

Hydrol. Earth Syst. Sci. Discuss., https://doi.org/10.5194/hess-2018-286
Manuscript under review for journal Hydrol. Earth Syst. Sci.
Discussion started: 12 July 2018

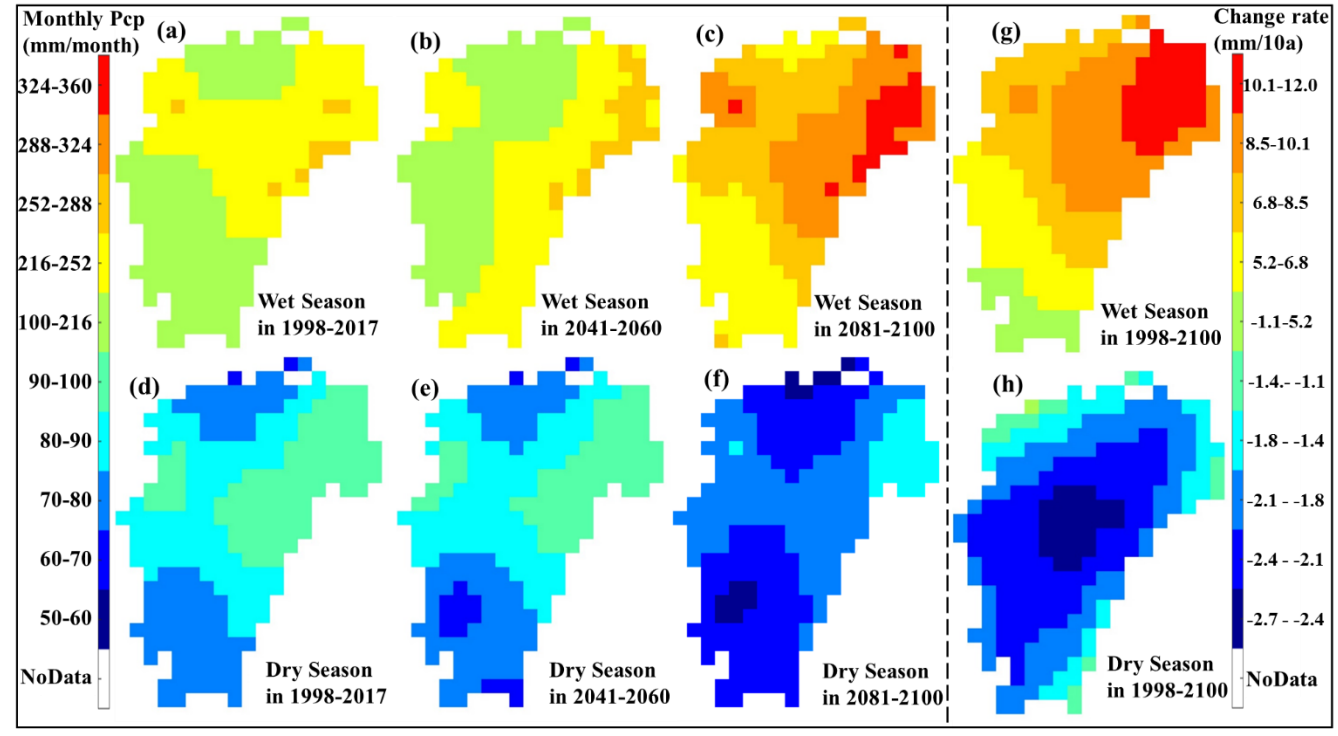

Fig. 9. The precipitation changes in the spatial pattern during the period from 1998 to 2100: average monthly precipitations of the wet season (April to July) during the historical period from 1998 to 2017 (a), 2041 to 2060 (b), and 2081 to 2100 (c); average monthly precipitations of the wet season (April to July) during the historical period from 1998 to 2017 (d), 2041 to 2060 (e), and 2081 to 2100 (f); change rate of monthly precipitation in wet (g) and dry (h) season from 1998 to 2100.

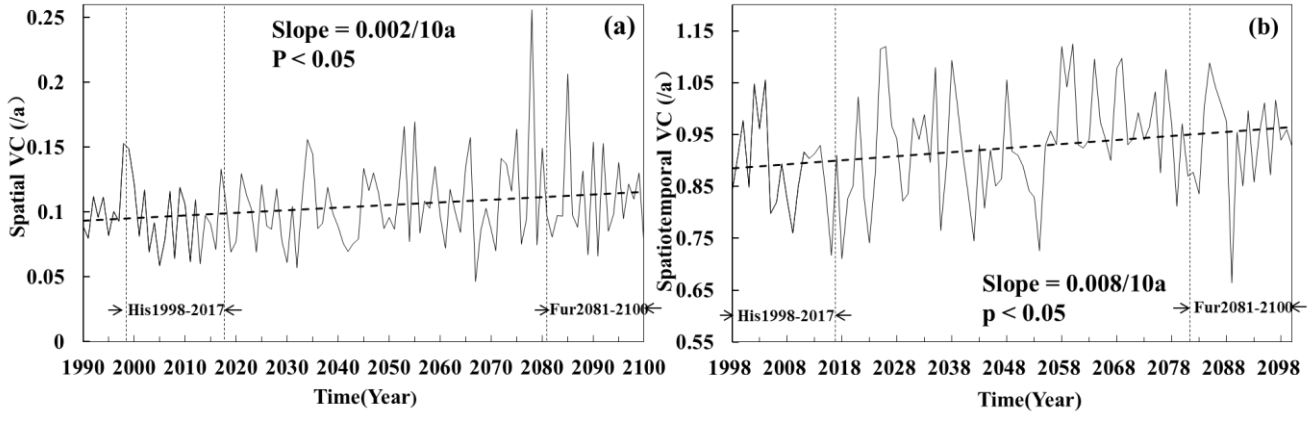

Hydrol. Earth Syst. Sci. Discuss., https://doi.org/10.5194/hess-2018-286
Manuscript under review for journal Hydrol. Earth Syst. Sci.
Discussion started: 12 July 2018

Hydrology and Earth System Sciences
Discussions

614 Fig. 10. The spatial (a) and spatiotemporal (b) variation coefficient for each year over 1988 to 2100. The far future period from
615 2081 to 2100 (Fur2081-2100) and baseline period from 1998 to 2017 (His1998-2017) are indicated by arrows.

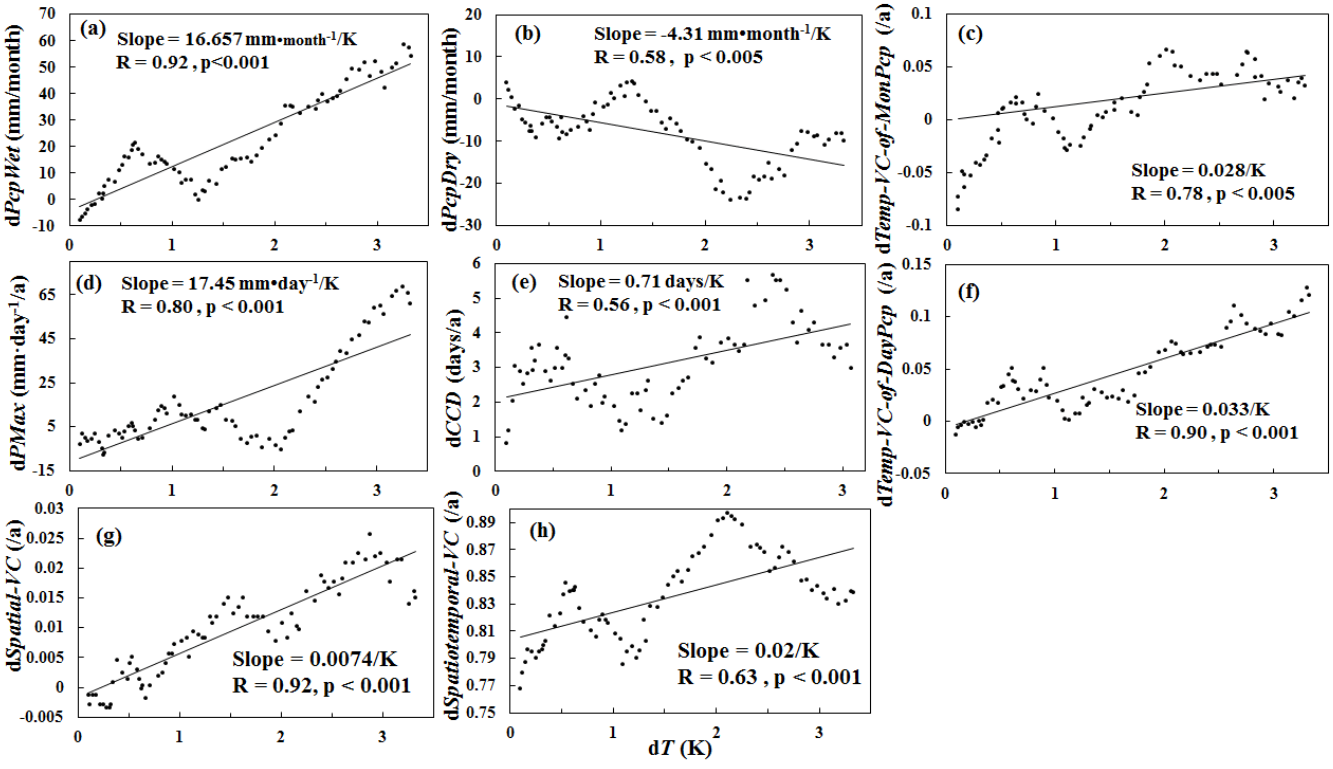

616

617 Fig. 11. The relationship between precipitation indexes changes (d*PcpIndex*) and temperature changes (d*T*). The precipitation
618 indexes include annual precipitation in the wet season (PcpWet) (a), annual precipitation in the dry season (PcpDry) (b),
619 temporal variance coefficient of monthly precipitations (Temp-VC-of-MonPcp) (c), annual max daily precipitation (PMax)
620 (d), annual max continual dry days (CCD) (e), temporal variance coefficient of daily precipitations (Temp-VC-of-DayPcp) (f),
621 spatial variance coefficient (Spatial-VC) (g), and spatiotemporal variance coefficient (Spatiotemporal-VC) (h). All the
622 precipitation index changes show significant correlations with temperature increases.